Cerebral Cortex December 2010;20:2818–2831
doi:10.1093/cercor/bhq028
Advance Access publication March 8, 2010

Pathway-Specific Utilization of Synaptic Zinc in the Macaque Ventral Visual Cortical Areas

Noritaka Ichinohe[1,2,3], Atsuko Matsushita[1], Kazumi Ohta[1] and Kathleen S. Rockland[1,4,5]

[1]Laboratory for Cortical Organization and Systematics, Brain Science Institute, RIKEN, Wako-shi, Saitama 351-0198, Japan, [2]Department of Advanced, International Medicine, Graduate School of Medicine, Kyoto University, Kyoto 606-8501, Japan, [3]Department of Neuroanatomy, Graduate School of Medicine, Hirosaki University, Hirosaki 036-8562, Japan and [4]Division of Neural Systematics, National Institute for Physiological Sciences, Okazaki, Aichi 444-8585, Japan

[5]Current address: The RIKEN-MIT Center for Neural Circuit Genetics, Howard Hughes Medical Institute, Department of Biology and Department of Brain and Cognitive Sciences, Massachusetts Institute of Technology, Cambridge, MA 02139, USA

Address correspondence to Noritaka Ichinohe, Laboratory for Cortical Organization and Systematics, Brain Science Institute, RIKEN, 2-1 Hirosawa, Wako-shi, Saitama 351-0198, Japan. E-mail: nichinohe@brain.riken.jp.

Synaptic zinc is an activity-related neuromodulator, enriched in hippocampal mossy fibers and a subset of glutamatergic cortical projections, exclusive of thalamocortical or corticothalamic. Some degree of pathway specificity in the utilization of synaptic zinc has been reported in rodents. Here, we use focal injections of the retrograde tracer sodium selenite to identify zinc-positive (Zn+) projection neurons in the monkey ventral visual pathway. After injections in V1, V4, and TEO areas, neurons were detected preferentially in several feedback pathways but, unusually, were restricted to deeper layers without involvement of layers 2 or 3. Temporal injections resulted in more extensive labeling of both feedback and intratemporal association pathways. The Zn+ neurons had a broader laminar distribution, similar to results from standard retrograde tracers. After anterograde tracer injection in area posterior TE, electron microscopic analysis substantiated that a proportion of feedback synapses was colabeled with zinc. Nearby injections, Zn+ intrinsic neurons concentrated in layer 2, but in temporal areas were also abundant in layer 6. These results indicate considerable pathway and laminar specificity as to which cortical neurons use synaptic zinc. Given the hypothesized roles of synaptic zinc, this is likely to result in distinct synaptic properties, possibly including differential synaptic plasticity within or across projections.

Keywords: feedback, feedforward, subpopulations of pyramidal neurons, ventral visual pathway, zinc

Introduction

Neurochemically, the overwhelming majority of cortical pyramidal neurons use glutamate as neurotransmitter. A subset, however, is distinguished by using synaptic zinc as cofactor. The density of zinc-positive (Zn+) terminations is area dependent, being least in primary areas and greatest in limbic-associated areas (Pérez-Clausell 1996; Frederickson et al. 2000, 2005; Ichinohe and Rockland 2004). In all areas, the middle layer is zinc poor (Pérez-Clausell 1996; Ichinohe and Rockland 2005; Wong and Kaas 2008). This is consistent with the fact that thalamocortical terminations do not contain zinc (Brown and Dyck 2004; Ichinohe et al. 2006). An additional implication is that feedforward cortical connections terminating in layer 4 are zinc negative. From this, more particularly, the question arises of whether there is pathway specificity as to which neurons use synaptic zinc, for example, among the feedforward, feedback, and lateral corticocortical projection.

Synaptic zinc is an activity- and calcium-dependent neuromodulator, known to interact with receptors, ion channels, and neurotrophic factors (for review, see Smart et al. 2004; Frederickson et al. 2005; Nakashima and Dyck 2009, Paoletti et al. 2009; Sensi et al. 2009). Thus, a preferential association of synaptic zinc with specific projections or subpopulations would be expected to impact on synaptic properties, including synaptic plasticity.

In most cortical areas, Zn+ terminations form 2 dense bands, one in layers 1b, 2, and upper 3 and another in the deeper layers (Pérez-Clausell 1996; Ichinohe and Rockland 2005). This distribution at least partly corresponds to that of feedback connections (Rockland and Pandya 1979; Maunsell and Van Essen 1983; Felleman and Van Essen 1991). In rodents, furthermore, retrograde tracing experiments demonstrate that Zn+ neurons are concentrated in layers 2, upper 3, and 6 (Garrett et al. 1992; Casanovas-Aguilar et al. 1998; Brown and Dyck 2005). The pathway-specific sources of Zn+ terminations are less investigated in the macaque cortex. We therefore set out to investigate whether synaptic is preferentially used by feedback projections.

Here, we used focal injections of sodium selenite to identify neurons giving rise to Zn+ terminations, within the ventral visual pathway of macaque monkeys, that is, V1, V4, TEO, and anterior temporal areas (see Materials and Methods, Sodium Selenite and BDA Injection). In fact, we find that feedforward projections, in contrast to feedback or lateral projections, tend to be zinc negative. More surprisingly, we also demonstrate a laminar dissociation within the early visual feedback projections, where projecting neurons in layer 6, but not in layer 2, are Zn+.

Materials and Methods

Experimental Subjects

Ten adult macaque monkeys (*Macaca mulatta* and *Macaca fuscata*) were used in this study: 9 were used for sodium selenite injections and one for electron microscopic (EM) analysis of anterogradely labeled Zn+ terminations. Three additional animals, used in other studies (in preparation), received sodium selenite injections in temporal cortex with variable survival times (40–48 h) in order to confirm the optimal postinjection survival times. All experimental protocols were approved by the Experimental Animal Committee of the RIKEN Institute and conformed to the National Institutes of Health (NIH) Guide for the Care and Use of Laboratory Animals (NIH Publications No. 80-23; revised 1996). Every effort was made to minimize the number of animals used and any pain or discomfort experienced by them.

Sodium Selenite and BDA Injection

There are 2 techniques for demonstrating Zn+ neurons. One is intraperitoneal injection of sodium selenite (Na_2SeO_3). This substance interacts with synaptic zinc to form precipitates of ZnSe, and in this form, it is transported retrogradely to the soma (Christensen et al. 1992; Casanovas-Aguilar et al. 2002). After histological processing, it reveals all Zn+ neurons (Slomianka et al. 1990; Brown and Dyck 2003). An alternative second method, used here, is to make focal injections of sodium selenite. Focal injections are less toxic in primates and have the further advantage of selectively labeling only those Zn+ neurons that project to the injection site (Christensen et al. 1992; Casanovas-Aguilar et al. 1995, 1998; Brown and Dyck 2005).

For 9 of the 10 monkeys, 0.5–0.7% of the retrograde tracer sodium selenite (Na_2SeO_3; Sigma; diluted in 0.9% NaCl) was injected into V1 (n = 2), V4 (n = 2), TEO (n = 1), or temporal cortical (n = 4) areas in order to visualize neurons giving rise to the Zn+ terminations in each of these areas. The 4 animals with temporal injections have been used in a previous report (Ichinohe and Rockland 2005), and injection localization is mapped in figure 3 of that report. Designations of subdivisions within temporal cortex are further described below and under "Nomenclature."

Surgery was carried out under sterile conditions after the animals were deeply anesthetized with barbiturate anesthesia (35 mg/kg Nembutal, intravenously [i.v.], after a tranquilizing dose of 11 mg/kg ketamine, intramuscularly [i.m.]). Cortical areas of interest were localized by direct visualization, subsequent to craniotomy and durotomy, in relation to sulcal landmarks (i.e., inferior occipital, lunate, superior temporal, and anterior or posterior middle temporal sulci). Pressure injections of sodium selenite were made by a 10-μL Hamilton syringe in regions corresponding to V1, V4, TEO, posterior dorsal TE (TEpd), anterior dorsal TE (TEad), anterior ventral TE (TEav), and the border of TEav and perirhinal cortex. Temporal area designations follow Yukie et al. (1990), Saleem and Tanaka (1996), Saleem et al. (2007), and Saleem and Logothetis (2007). In one V1 case (R63), 3 injections were made (each 1.0 μL), each separated by about 2.0 mm. The other 8 brains all received one injection (volume 1.0–1.5 μL). This resulted in histological injection sites of 1.5–2.0 mm in diameter (Fig. 1; fig. 3 in Ichinohe and Rockland 2005). All histological injection sites were through all cortical layers (Fig. 1; fig. 3 in Ichinohe and Rockland 2005). Injections aimed at V2 resulted in significant involvement of adjacent V1 and not included in the analysis.

In one monkey, biotinylated dextran amine (BDA; Molecular Probes) was injected in area TEpd for subsequent EM analysis of pathway-specific Zn+ boutons, anterogradely labeled by BDA (see below). Two injections (1.0 μL each) of 10% solution (1:1 mixture of 3000 and 10 000 MW) in 0.0125 M phosphate-buffered saline (PBS: pH 7.4) were made.

Visualization of Zn+ Projection Neurons

A postinjection survival of 24 h was used, consistent with previous experiments in rodents (Christensen et al. 1992; Casanovas-Aguilar et al. 1995, 1998) and primates (Ichinohe and Rockland 2005). The efficacy of the survival time was evaluated by several features of the resulting projections. 1) We successfully identified, in our material, projections that were 1.8–2.1 cm from the injection site; for example, Zn+ neurons in the posterior hippocampus were labeled by injections in TEav (see also, Ichinohe and Rockland 2005), and neurons in the temporal pole were labeled after injections in TEpd (case 66). 2) As a further control, longer survivals (40–48 h) were tested in 3 animals used in other experiments. The longer postinjection survivals produced more necrosis and less intense labeling around the injection site, with no detectable enhancement in either the local or long distance connections. Because a negative trend was already evident with longer survival times (comparing 20–24 h vs. 40–48 h), we did not extend postinjection survival times beyond 48 h, but the expectation is that, like horseradish peroxidase, the retrogradely transported sodium selenite would be cleared from the neurons with longer survival times.

After injection and recovery, the animals were re-anaesthetized (11 mg/kg, i.m. katamine: ketamine followed by 75 mg/kg, intraperitoneally Nembutal) and then perfused transcardially, in sequence, with saline containing 0.5% sodium nitrite; 4% paraformaldehyde in 0.1 M phosphate buffer (PB) for 30 min; and chilled 0.1 M PB with 10%, 20%, and 30% sucrose. The brains were removed from the skull, blocked, and immersed into 30% sucrose in 0.1 M PB. The brains were cut in the coronal plane by frozen microtomy (at 50 μm thickness), and tissue was collected in repeating series. The series consisted of: zinc, thionin, and parvalbumin, with 1 or 2 sections reserved or discard. Sections were washed thoroughly with 0.1 M PB, followed by 0.01 M PB. The IntenSE M silver Enhancement kit (Amersham International) was used, 1:1 with 33% gum arabic solution, to intensify zinc signals (Danscher et al. 1987; De Biasi and Bendotti 1998). Development of reaction products was monitored under a microscope and terminated by rinsing the sections in 0.01 M PB and, subsequently, several rinses in 0.1 M PB. Precipitate, interpreted as the reaction product (zinc selenite) of injected selenium with Zn^{2+} at the injection site, was formed within cell somata, consistent with previous reports (Christensen et al. 1992;

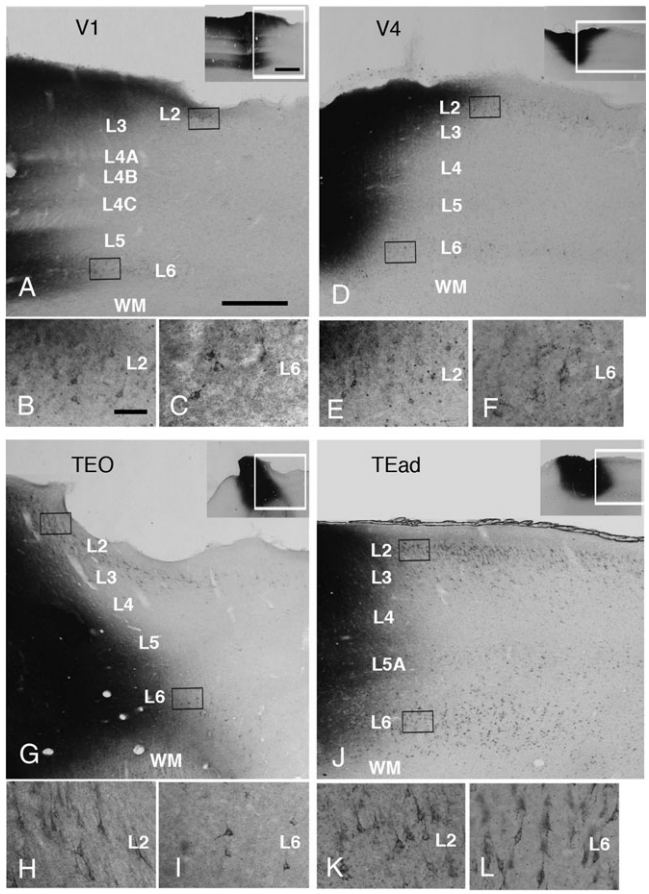

Figure 1. Sodium selenite injection sites from 4 different areas and intrinsic Zn+ neurons in the immediate vicinity of the injections. (*A*) Low magnification of the injection in case 63 (area V1), from boxed area in the inset, where the injection is shown at lower magnification. The section has been chosen from the edge of the injection, where the tracer does not fully extend through the full cortex. (*B*) Higher magnification of labeled neurons in layer 2, from upper box in (*A*). (*C*) Higher magnification of labeled neurons in layer 6, from lower box in (*A*). (*D*) Low magnification of the injection in case 286 (area V4), from boxed area in the inset, where the injection is shown at lower magnification. (*E*) Higher magnification of labeled neurons in layer 2, from upper box in (*D*). (*F*) Higher magnification of labeled neurons in layer 6, from lower box in (*A*). (*G*) Low magnification of the injection in case 314 (area TEO), from boxed area in the inset, where the injection is shown at lower magnification. (*H*) Higher magnification of labeled neurons in layer 2, from upper box in (*G*). (*I*) Higher magnification of labeled neurons in layer 6, from lower box in (*G*). (*J*) Low magnification of the injection in case R62 (area TEad), from boxed area in the inset, where the injection is shown at lower magnification. (*K*) Higher magnification of labeled neurons in layer 2, from upper box in (*J*). (*L*) Higher magnification of labeled neurons in layer 6, from lower box in (*J*). Scale bar: *A*, *D*, *G*, *J*, and insets in each figure, 500 μm; *B*, *C*, *E*, *F*, *H*, *I*, *K*, *L*, 100 μm.

Casanovas-Aguilar et al. 1998; Ichinohe and Rockland 2005). Some sections were double processed for Nissl substrate using NeuroTrace 500/525 green fluorescent Nissl stain (Molecular Probes) according to the company's protocol. Parvalbumin sections were reacted by standard procedures, as described in Ichinohe and Rockland (2005).

EM Analysis of Boutons Containing Zn and BDA

After the BDA injections, the animal was allowed to recover and survived 22 days. As a terminal procedure, the animal was deeply anesthetized and then injected i.v. with saline containing 10% sodium sulfide (200 mg/kg). Two minutes after the injection, the animal was perfused transcardially, in sequence, with saline containing 0.5% sodium nitrite, 4% paraformaldehyde with 0.1% glutaraldehyde in 0.1 M PB for 30 min, and chilled 0.1 M PB with 10% and then 20% sucrose. The brain was removed from the skull, and 2 small cortical blocks were excised and kept in 0.1 M PB. Block 1, trimmed in an oblique coronal plane, included areas TEO and V4, respectively, ventral and dorsal to the inferior occipital sulcus. Block 2 was slightly posterior, oriented in the horizontal plane, and included V1, V2, V4, and the adjacent posterior bank of the superior temporal sulcus (STS).

Vibratome-cut sections (50 μm thick) were prepared and washed thoroughly with 0.1 M PB, followed by 0.01 M PB. For each block, a repeating series of 4 consecutive sections was collected in 4 groups (A–D). Group C was first prepared for light microscopic examination of BDA only in order to identify regions with dense BDA label. These sections were incubated in 0.5% Triton-X 100 in 0.1 M PBS for 30 min, followed by avidin–biotin complex (VECTASTAIN Elite ABC, Vector Labs) containing 0.5% Triton-X 100 overnight (17–24 h). In the final step, BDA was demonstrated by 3,3′-diaminobenzidine tetrahydrochloride (DAB) histochemistry.

After we identified BDA-dense regions, we selected several adjoining sections in the B and D groups. These were double-reacted, first for zinc and then for BDA. The IntenSE M silver Enhancement kit, mixed 1:1 with the same amount of 33% gum arabic, was used to intensify zinc signals as described above. Development was terminated by rinsing the sections in water. The zinc enhancing time was 2.5 and 3 h for B and D, respectively. (Series A was used to test technical parameters and/or held in reserve.) Sections were further processed for peroxidase histochemistry for BDA as described above, but with Triton-X 100 at 0.03% instead of 0.5%. The sections double-labeled for zinc and BDA were then osmicated, dehydrated, and flat-embedded in Araldite resin (TAAB). From the plastic sections, we identified and further trimmed out small regions where dense BDA-labeled terminals overlapped with a dense stratum of Zn+ terminations. Semiserial silver sections were collected on formvar-coated, single-slot grids; contrasted with 4% uranyl acetate; and examined with an electron microscope (JEM 2000-EX; JEOL). Five to 10 ultrathin sections from selected brain areas (TEO, V4, STS, and V1; see Table 1) were surveyed for BDA and Zn+ profiles at low magnifications (×5000 to ×10 000). When candidate BDA+/Zn+ or BDA+/Zn-negative profiles were identified, electron micrographs were taken at magnifications of ×50 000 for detailed observation.

Table 1
BDA+/Zn+ or BDA+/Zn-negative feedback synapses

EM block	Dimension of surveyed field including L1/L2 (mm^2)[a]	Number of ultrathin sections analyzed	Location	Total	BDA+/ Zn+	BDA+/ Zn-negative
1D5a (3 h[b])	1 × 0.5	10	TEO	5	1	4
1D5b (3 h[b])	0.7 × 0.35	10	TEO	7	3	4
1B5a (2.5 h[b])	1 × 0.75	5	TEO	7	3	4
1D20a (3 h[b])	1 × 0.5	5	V4	15	6	9
2B3 (2.5 h[b])	0.5 × 0.5	6	V1	5	4	1
2D6a (3 h[b])	0.75 × 0.6	8	STS	10	6	4

[a]The first number is length, measured parallel to the pia; second number is depth from pia.
[b]Incubation time for zinc enhancing.

Data Analysis

Retrogradely labeled cells were plotted using a computer-aided microscope system and the Neurolucida software package (MicroBrightfield). The microscope (E800; Nikon) was equipped for fluorescent and dark field microscopy. The outline of the section and laminar boundaries was added to the plots by referring to fluorescence Nissl or adjacent thionin-stained sections.

Photomicrographs were taken with a digital camera (Axioscop2 and Axiocam; Carl Zeiss Vision). Images were saved in TIFF format and imported into Adobe Photoshop CS4. Image brightness, contrast, and color were adjusted as necessary to reproduce the original histological data.

Additional experimental tissue from several previous experiments was available. This included 2 brains perfused for synaptic zinc (Ichinohe and Rockland 2005), 3 brains with injections of cholera toxin B-subunit conjugated to Alexa 488 or Alexa 594 in temporal areas (Borra et al. 2010), and 4 brains injected with BDA (Ichinohe et al. 2008).

Nomenclature

Areas V1, V4, and TEO were identified by reference to sulcal landmarks, in comparison with published maps, and by architectonic analysis of selected histological sections stained for cell bodies or parvalbumin (Saleem and Logothetis 2007; Ungerleider et al. 2008; Borra et al. 2010). Subdivisions within the inferotemporal region are more variable between individual monkeys and tend not to have sharp borders (Zeki 1996). In placing injections, we targeted 3 major subdivisions, defined in relation to the posterior and anterior middle temporal sulci, namely TEpd, TEad, and TEav. A forth injection was at the border of TEav and perirhinal cortex. This nomenclature follows that of Yukie et al. (1990), Saleem and Tanaka (1996), Saleem et al. (2007), and Saleem and Logothetis (2007), with reference to that of Suzuki and Amaral (2003a, 2003b). Foci of Zn+ neurons are described within area TF, TH, TG, and smaller subdivisions of TE within or near the STS (TEm, TEa, and TPO). These are designated with reference to Saleem and Logothetis (2007) and Seltzer and Pandya (1989) and marked on the section outlines in Figures 5, 6, 7, and 9.

In referring to zinc-enriched terminals and neurons, we have for convenience used the shorter designation Zn+ (= zinc positive). We avoided the descriptor "zincergic" as we are taking a conservative stance that further criteria are needed before these populations can be accepted as distinct types.

Results

Zn+ Neurons Nearby the Injection Sites

Injections in all our targeted areas produced Zn+ neurons in the vicinity of the injection, but marked area-specific differences were apparent in the laminar distribution and density (Fig. 1). In area V1, there were relatively few Zn+ neurons. These were mainly in layer 2 and were restricted to the immediate vicinity of the injection site (less than 0.7 mm from the injection edge; Fig. 1*A,B*). A few Zn+ neurons were observed in layer 6 (Fig. 1*C*). Injections in V4 or TEO also produced Zn+ neurons mainly in layer 2 (Fig. 1*D,E,G,H*), but, compared with the labeling after injections in V1, the Zn+ neurons extended further from the edge of the injection (up to 1.0 mm). Some Zn+ neurons occurred in layer 6, in the immediate vicinity of the injections (Fig. 1*D,F,G,I*).

The distribution of Zn+ neurons was conspicuously different in the temporal cases (Fig. 1*J,K,L*). First, more layers were involved. Numerous Zn+ neurons occurred not only in layer 2 but also in layer 6 and, to a lesser extent, in upper layer 3 and layer 5. Second, the bands of Zn+ neurons extended further from the edge of the injection, up to 1.5–2.0 mm. None of these Zn+ intrinsic connections had any discernible patchiness. We note, however, that the sparse label in layer 3 of temporal areas exhibited some periodic fluctuation. The number of labeled

neurons near the injection site increased from V4 and TEO to TEad (see Fig. 1).

Zn+ Extrinsic Cortical Projections: Areas V1, V4, and TEO

In this section and the following section, we begin with a brief summary of the main projections, as reported by others from standard retrograde tracers, that is, wheat germ agglutinin conjugated with horseradish peroxidase, fluorescent dyes, or cholera toxin conjugates, see also Figure 11. This is intended as aid in the interpretation of zinc-specific patterns. We continue to use the nomenclature of "feedforward" projections to designate projections originating mainly from layer 3 and terminating mainly in layer 4. "Feedback" projections designate those avoiding layer 4, terminating mainly in layer 1, or in layers 1 and 6, and originating mainly from neurons in layers 6, 2, and upper 3 (Rockland and Pandya 1979; Maunsell and Van Essen 1983; Felleman and Van Essen 1991; Born and Bradley 2005; Sincich and Horton 2005; Ungerleider et al. 2008). As repeatedly discussed in the literature, classification criteria are not always clear, and especially, connections between higher order areas can be hard to classify with the available criteria. In general, what have been called "association," "intermediate," or "lateral" connections originate from and terminate in more layers (Rockland and Pandya 1979; Maunsell and Van Essen 1983; Felleman and Van Essen 1991; Ungerleider et al. 2008).

Standard Tracers (Area V1)

Cortical projections to area V1 originate from areas V2, V3, V4, MT, several smaller areas in the STS and intraparietal sulcus (IPS), and sporadically from areas TEO, TE, parahippocampal gyrus, and frontal eye fields (Maunsell and Van Essen 1983; Distler et al. 1993; Rockland et al. 1994; Barone et al. 2000). These are all feedback projections. Labeled neurons are in layers 2, upper 3, and 6, or in layer 6 alone for the more distant foci, such as in TEO and TE (Doty 1983; Rockland and Van Hoesen 1994; Barone et al. 2000).

Sodium Selenite (Area V1)

Of areas reviewed above, only 2 foci contained Zn+ neurons, one in the depth of the lunate sulcus (area V2: Fig. 2*A,B*) and the second in the lower bank of the STS (area MT: Fig. 2*C,D*). In marked contrast to standard tracers, labeled neurons were only in layer 6 and not in layers 2 and 6.

Standard Tracers (Area V4)

Cortical projections to V4 differ slightly, depending on whether the injection is placed in the central or peripheral visual field representation (for review, see Barone et al. 2000; Ungerleider et al. 2008). Major projections are from area V2 (feedforward, with neurons predominantly in layer 3); from areas V3A, V4t, MT, and DP (intermediate or lateral, originating from neurons in layers 3 and 5); and feedback from anterior areas in TE, TEO, the STS, IPS, and area TF in the parahippocampal gyrus. These latter originate from neurons in the deeper layers, with some involvement of layers 2 and uppermost 3 (Rockland and Pandya 1979; Felleman and Van Essen 1991). In addition, neurons in the frontal eye field project to V4 (Barone et al. 2000).

Sodium Selenite (Area V4)

Sodium selenite injections in area V4 produced label mainly in a subset of feedback connections (Figs 3 and 4), namely the most posterior STS (Fig. 3, section 81; Fig. 4*A,B*) and area TEO in the lower bank of the STS and the lateral bank of the occipitotemporal sulcus (OTS: Fig. 3, section 53). Surprisingly, Zn+ neurons were limited to layer 6. As remarks above, in contrast, standard tracers produce labeled neurons in the upper layers as well. After the more dorsal injection in V4, Zn+ neurons also occurred in the parahippocampal gyrus (not illustrated). These were in the deeper layers, in this instance, consistent with previous reports (Felleman and Van Essen 1991; Ungerleider et al. 2008).

The more ventral injection in V4 resulted additionally in a few neurons at the lateral edge of the annectant gyrus (area V3A: Fig. 3, sections 81 and 90; Fig. 4*C,D*). This has been described as an "intermediate-type" projection (Ungerleider et al. 2008), although the Zn+ neurons were mainly in layer 6.

Standard Tracers (Area TEO)

Cortical projections to area TEO (Rockland and Pandya 1979; Distler et al. 1993) include those from areas V2, V3, V4, and, more sparsely, MT (feedforward); from FST in the STS and from parietal area LIP (intermediate); and from area TE, areas in the anterior STS, parahippocampal area TH, perirhinal area 36, and TG (feedback: Distler et al. 1993; Lavenex et al. 2002). The peripheral field representation, located more ventrally (and not injected by us), receives several additional projections (Distler et al. 1993).

Sodium Selenite (Area TEO)

In contrast with standard tracers, it is again apparent that only a subset of projections are Zn+, and these corresponded closely to the feedback projections. A small focus of Zn+ neurons was found in the perirhinal cortex (Fig. 5, section 118). Other foci were detected in the lower bank of the anterior STS (TEa and possibly IPa: Fig. 5, section 92) and in the parahippocampal gyrus (area TF: Fig. 5, sections 63 and 82). Except for the parahippocampal gyrus, these had a bilaminar distribution but were denser in layer 6. From the vicinity of the injection, dense label extended about 10 mm anterior, well into area TE and adjoining perirhinal cortex (Fig. 5, sections 74, 82, 92, and 118). At these levels, consistent with previous descriptions of feedback connections, label was predominantly in layer 6. Posterior to the injection, the field of labeled neurons extended 4.0 mm, within what is probably still area TEO (Fig. 5, section 44). Labeled neurons were in both the supra- and infragranular layers, as would be expected for intrinsic or lateral connections.

Zn+ Extrinsic Cortical Projections: Temporal Areas

Standard Tracers

The projections to perirhinal cortex and the various subdivisions of area TE have been extensively investigated (Yukie et al. 1990; Baizer et al. 1991; Webster et al. 1991, 1994; Distler et al. 1993; Suzuki and Amaral 1994; Saleem et al. 1993, 2000, 2007; Saleem and Tanaka 1996; Kondo et al. 2005) and will only be summarize here. Main projections include those from posterior unimodal visual areas (V4 and TEO), from several areas in the STS, from temporal polar cortex, and (for TE) from perirhinal cortex. Projections from the unimodal visual areas can be considered feedforward. Other projections have a bilaminar distribution of efferent neurons in the supra- and infragranular layers, a pattern consistent with intermediate or lateral connections (Yukie et al. 1990; Webster et al. 1991, 1994;

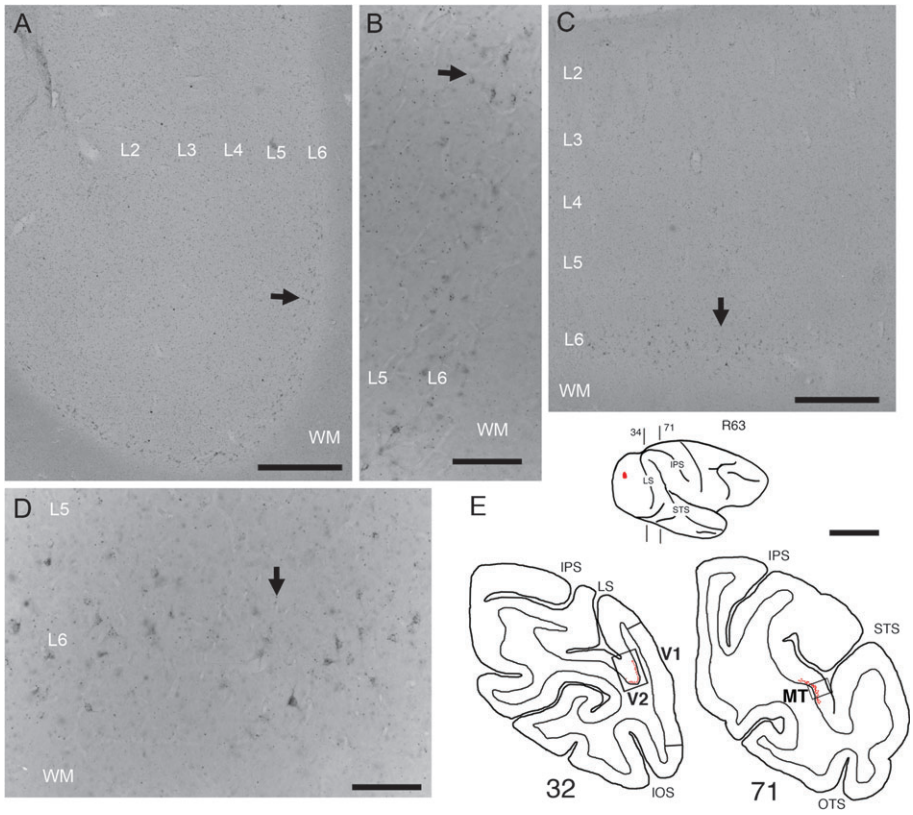

Figure 2. Two fields of Zn+ neurons, retrogradely labeled by an injection of sodium selenite in area V1. (*A*) Neurons in layer 6 of the lunate sulcus (area V2). An image is from rectangle part in (*E*) section 32. (*B*) Higher magnification from the arrow in (*A*). (*C*) Neurons in layer 6 of the STS (area MT). An image is from rectangle part in (*E*) section 71. (*D*) Higher magnification from the arrow in (*C*). (*E*) Schematic right hemisphere (case R63) and 2 coronal section outlines (where larger numbers are more anterior) showing the location of the injection site in area V1 (red spot) and the location of Zn+ neurons (in red; one dot = one neuron). The anterior-posterior position of the sections is indicated by the interrupted lines drawn on the right hemisphere schematic, at the top of the figure. The lines are numbered to correspond to the respective sections. IOS, inferior occipital sulcus; LS, lunate sulcus; V1, area V1; V2, area V2; MT, area MT. Scale bar: *A*, *C*, 500 μm; *B*, *D*, 100 μm; *E*, 5 mm.

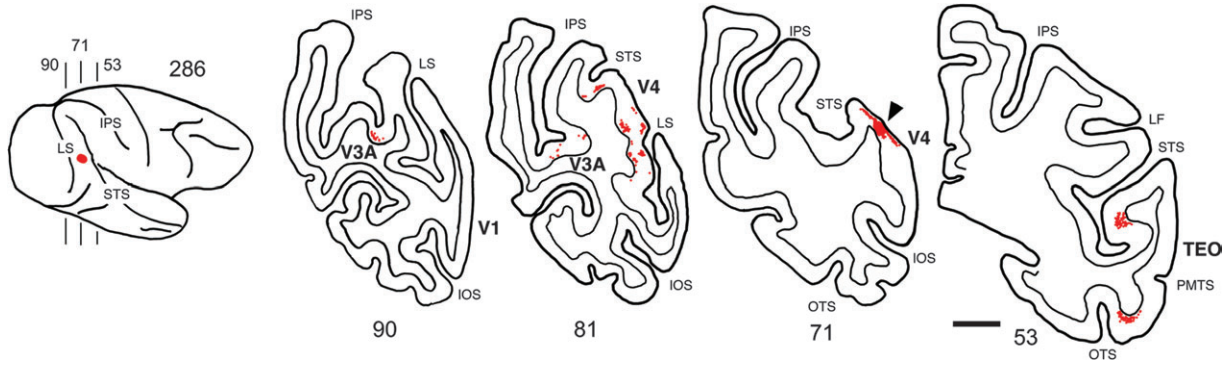

Figure 3. Schematic right hemisphere (case 286) and 4 coronal section outlines (where larger numbers are more posterior) showing the location of the injection site in area V4 (red spot and arrowhead in section 71) and the location of Zn+ neurons (in red; one dot = one neuron). Other conventions are the same as in Figure 2*E*. LF, lateral fissure; PMTS, posterior medial temporal sulcus; TEO, area TEO; V3A, area V3A; V4, area V4; others, see Figure 2*E*. Scale bar, 5 mm.

Martin-Elkins and Horel 1992; Distler et al. 1993; Saleem et al. 1993, 2000; Suzuki and Amaral 1994; Saleem and Tanaka 1996).

Sodium Selenite

Four injections were placed in different locations within TE. The distribution of Zn+ neurons in case 299, with an injection at the TEav/perirhinal border, is similar to that in case 295, where the injection was more lateral, confined to TEav without involvement of perirhinal cortex. The projections in case 295 are described but not illustrated.

In our material, there were few or no Zn+ neurons posterior to the injections, in what would correspond to feedforward projections (Figs 6–9). Notably, the expected feedforward projections from V4 and TEO were not labeled in any of the 4 cases. Major projection foci were detected in the OTS, in the

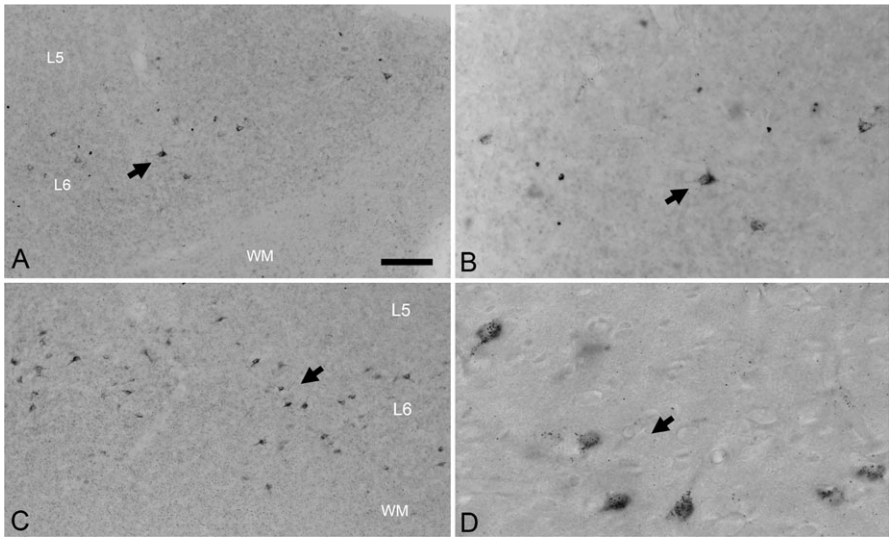

Figure 4. Two fields of Zn+ neurons, retrogradely labeled by an injection in area V4 (case 286, Fig. 3). (*A*) Zn+ neurons in layer 6 of the annectant gyrus (area V3A; see Fig. 3, sections 81 and 90). (*B*) Higher magnification, from arrow in (*A*). (*C*) Zn+ neurons in layer 6 of the posterior STS (area 7a; see Fig. 3, section 81). (*D*) Higher magnification, from the arrow in (*C*). Scale bar, *A*, *C*, 100 μm: *B*, 50 μm; *D*, 25 μm.

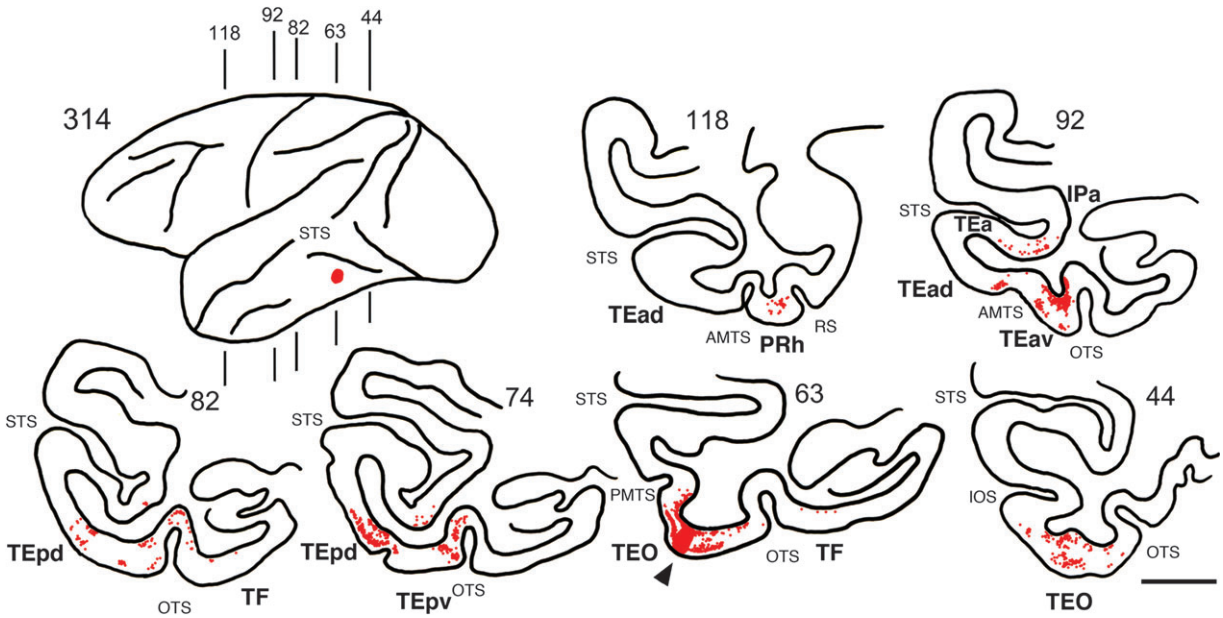

Figure 5. Schematic left hemisphere and 6 coronal section outlines (ventral part only) showing the location of the injection site in area TEO (case 314) and the distribution of Zn+ neurons. Larger numbers are more anterior. Other conventions are the same as in Figure 2*E*. AMTS, anterior medial temporal sulcus; IPa, area IPa; PRh, perirhinal cortex; RS, rhinal sulcus; TEa, area TEa; TEad, area TEad; TEav, area TEav; TEpd, area TEpd; TEpv, area TEpv; TF, area TF; others, see Figure 3. Scale bar, 5 mm.

parahippocampal gyrus, in several fields in the STS, and anterior to the injections.

Sodium Selenite: Projection Foci Posterior to the Injections

Some Zn+ neurons were detected in areas posterior to the injection (>4.0 mm), but these are likely to be within a subdivision of TE (Figs 6–9). In case R62 (TEad injection), there was a prominent posterior focus in the medial bank of the OTS (TEpv: Fig. 9, section 91). In case 299 (injection in TEav/perirhinal), there was also a posterior focus in the OTS, but in both its lateral and its medial banks (TEpv: Fig. 7, section 68; Fig. 8*A*). In case 295 (TEav injection, not illustrated, but see fig. 3 in Ichinohe and Rockland 2005), labeled neurons were similarly located in the depth and lateral bank of the OTS (TEpv). In these foci in the OTS, labeled neurons were predominantly in a bistratified distribution, but with a bias for the upper layers. In case R66 (TEpd injection), there was extensive bistratified labeling for about 2.0 mm posterior to the injection (Fig. 6, section 94). Because this is relatively close to the injection, this can be "intrinsic" and/or lateral (i.e., remaining within TEpd).

Sodium Selenite: Projection Foci in the Parahippocampal Gyrus

All 4 injections resulted in label in the parahippocampal gyrus. In case R62 (with the most anterior injection), this was

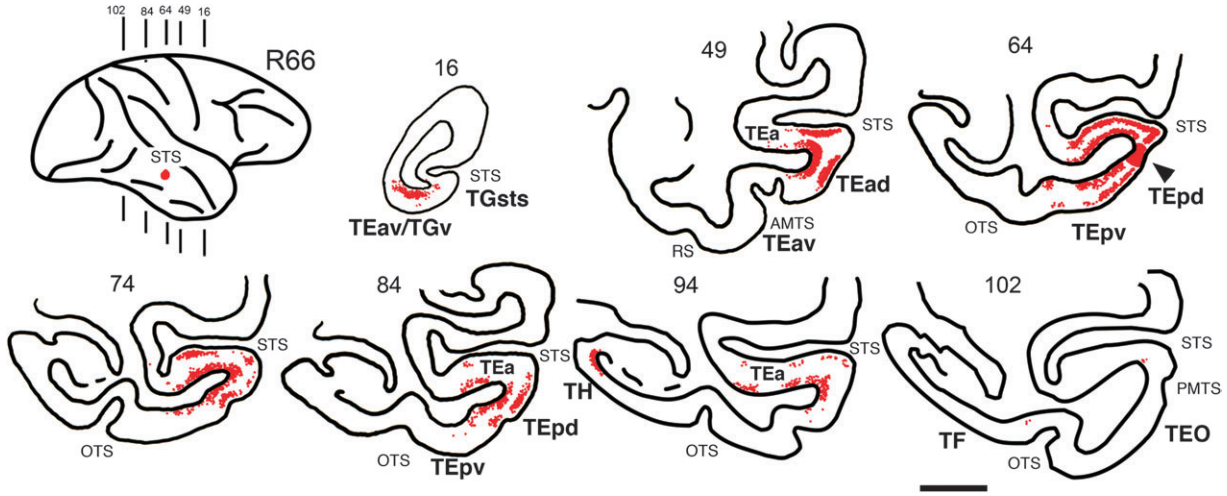

Figure 6. Schematic right hemisphere and ventral portion of 7 coronal section outlines showing the location of the injection site in area TEpd (case R66) and the distribution of Zn+ neurons. Larger numbers are more posterior. Other conventions are the same as in Figure 2*E*. Here and in Figures 7 and 9, the temporal pole is shown in isolation. AMTS, anterior medial temporal sulcus; PMTS, posterior medial temporal sulcus; TGsts, area TGsts; TGv, area TGv; TH, area TH; others, see Figure 5. Scale bar, 5 mm.

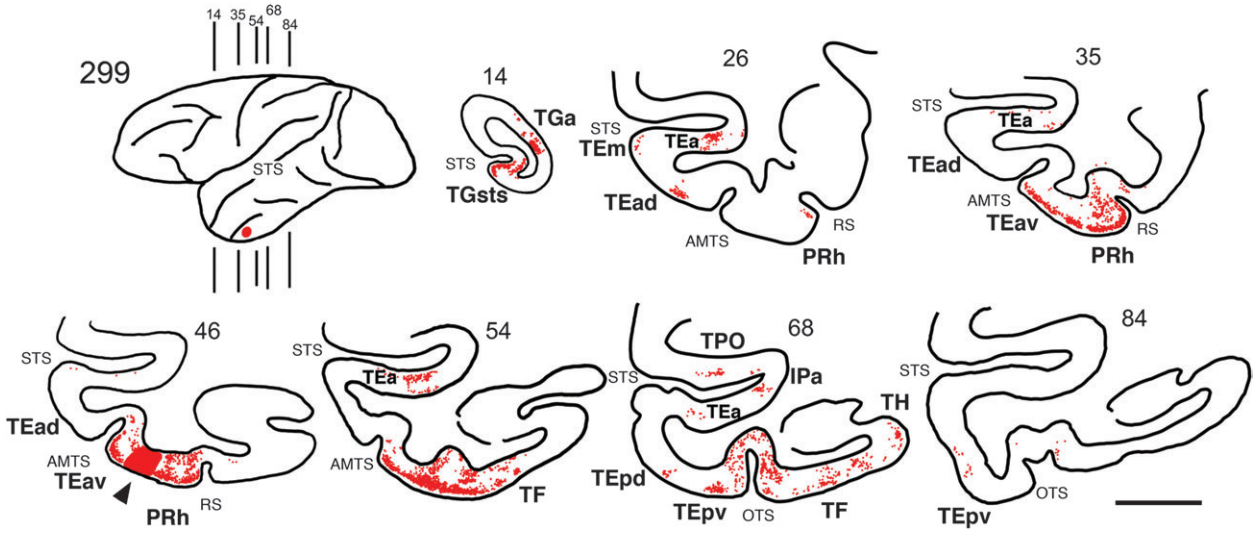

Figure 7. Schematic left hemisphere and ventral portion of 7 coronal sections showing the location of the injection site at the border of TEav and perirhinal cortex (case 299) and the distribution of Zn+ neurons. Larger numbers are more posterior. Other conventions are the same as in Figure 2*E*. TGa, area TGa; TPO, area TPO; others, see Figure 6. Scale bar, 5 mm.

relatively posterior, in TF and TH, and restricted to layer 6 (Fig. 9, sections 77 and 91). In case 299 (TEav/perirhinal injection), the focus was slightly more anterior, with the same layer 6 distribution but also upper layer involvement (Fig. 7, sections 54 and 68). In case 295 (TEav injection; not illustrated), the focus was similarly anterior (near the anterior tip of the OTS), but neurons were restricted to layer 6. In the posterior case of this series (R66), only a few scattered neurons occurred in area TF, but there was a distinct focus in area TH in layer 6 (Fig. 6, sections 94 and 102).

Sodium Selenite: Projection Foci in the STS

Projections from the STS were visualized from 2 foci, likely to be multimodal areas. In case 62 (with the most anterior injection), Zn+ neurons occurred in the upper bank of the STS (area TPO) and continued for about 6.0 mm (Fig. 9, sections 25, 35, and 45). These were located in the supra- and infragranular layers, except at the posterior fringe, where they were restricted to layer 6. After a gap of about 4.0 mm, a second group of Zn+ neurons appeared in the lower bank of the STS, in a bistratified distribution (Fig. 9, section 91; Fig. 10*C*). In case 299 (TEav/perirhinal injection), at anterior levels of the STS, Zn+ neurons were found in the lower bank (TEa), mainly in the upper layers, with a few neurons in layer 6 (Fig. 7, sections 26, 35, 54, and 68; Fig 8*B*). There were also a few neurons in layer 3 of the adjoining lip of the STS (TEm: Fig. 7, section 26). More posteriorly, Zn+ neurons occurred in the upper bank (TPO), depth (IPa), and lower bank (TEa: Fig. 7, section 68). These were mainly in the upper layers. In case 295 (TEav injection; not illustrated), there was a comparatively smaller number of Zn+ neurons. These were in the lower bank, anterior (TEa) and more posterior (TEm). Neurons in both foci were mainly in the upper layers. In the most posterior case (R66), the injection was immediately adjacent to the STS. This resulted in abundant

labeling in the STS, in a bistratified distribution, both anterior and posterior to the injection (Fig. 6, sections 49, 64, 74, 84, and 94). Given the proximity of the injection site, this projection could be mainly intrinsic but encompassing a further extrinsic component (Fig. 6, sections 84 and 94).

Sodium Selenite: Projection Foci Anterior to the Injection

In all 4 cases, Zn+ neurons were found anterior to the injection sites. In the immediate vicinity of the injections, these could be considered association connections, as described with standard retrograde tracers (Figs 6–9, 10*B*; Yukie et al. 1990; Fujita I and Fujita T 1996; Lavenex et al. 2004). In addition, labeled neurons occurred ventrally in the temporal pole (Figs 6, 7, 9, 10*A*), mainly in layers 2 and 6 (TEav/TGv and TGsts: Kondo et al. 2003; Saleem et al. 2007). The injection at the TEav/perirhinal border (case 299) produced Zn+ neurons more dorsomedially in the temporal pole (TGa: Kondo et al. 2003; Fig. 7, section 14). The anterior most injection (case R62) produced neurons dorsally (area TGd of Saleem et al. 2007; Fig. 9, section 12). The injection in area TEav (case 295, not illustrated) resulted in only a small number of Zn+ neurons in TGv.

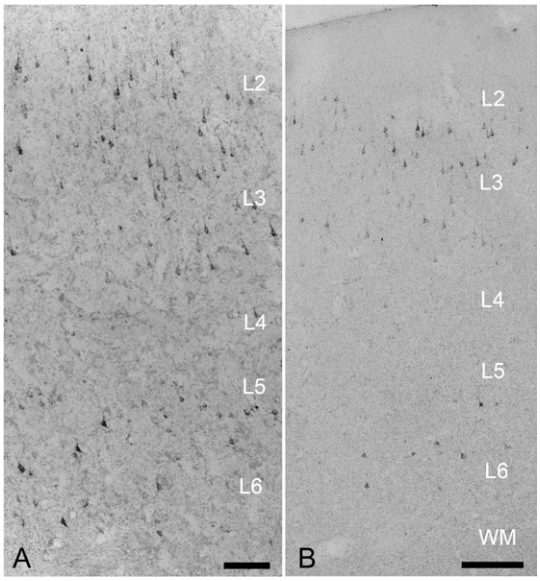

Figure 8. Two fields of Zn+ neurons, labeled by the injection in case 299. (*A*) Zn+ neurons in layers 2, 3, 5, and 6 in the medial bank of the OTS (area TEpv; Fig. 7, section 68). The ventral surface of the brain is at the top and medial to the left. (*B*) Zn+ neurons in layers 2, 3, and 6 of the lower bank of the STS (area TEa; Fig. 7, section 26). Scale bar: *A*, 100 μm; *B*, 200 μm.

EM Identification of Zn+ BDA-Labeled Cortical Projections

We prepared one brain with BDA injections in TEpd. The intention was to corroborate by another technique (BDA labeling), the finding that feedback and association projections can be Zn+. We did not carry out the same experiment for feedforward projections because of the evidence that these would be largely negative for zinc. That expectation was based on 1) the present sodium selenite results and 2) the relative absence of Zn+ terminations in the principal layers targeted by feedforward terminations.

Zn+ synapses were identified by the presence of large silver grains within a vesicle-containing profile (Fig. 12*D,E*). These Zn+ synapses derive from multiple sources, including callosal connections, extrinsic cortical projections not labeled by our BDA injection, intrinsic cortical connections, and amygdalo-cortical connections (Casanovas-Aguilar et al. 1995, 1998; Brown and Dyck 2005; Miyashita et al. 2007). Thus, Zn+ synapses alone were not included in our analysis.

BDA-labeled profiles were identified by the standard dark DAB reaction product. Synapses judged to be positive for both zinc and BDA were required to have an unambiguous colocalization of silver grains and DAB reaction product, together with distinct synaptic vesicles (Fig. 12*F–H*). Profiles where the vesicles were obscured or where the presence of DAB was ambiguous were not counted. Thus, some degree of under counting is likely. Fields were selected from the densest regions of BDA label, at the border of layers 1 and 2 (Fig. 12*A–C*). Some retrogradely filled neurons resulted from the BDA injections.

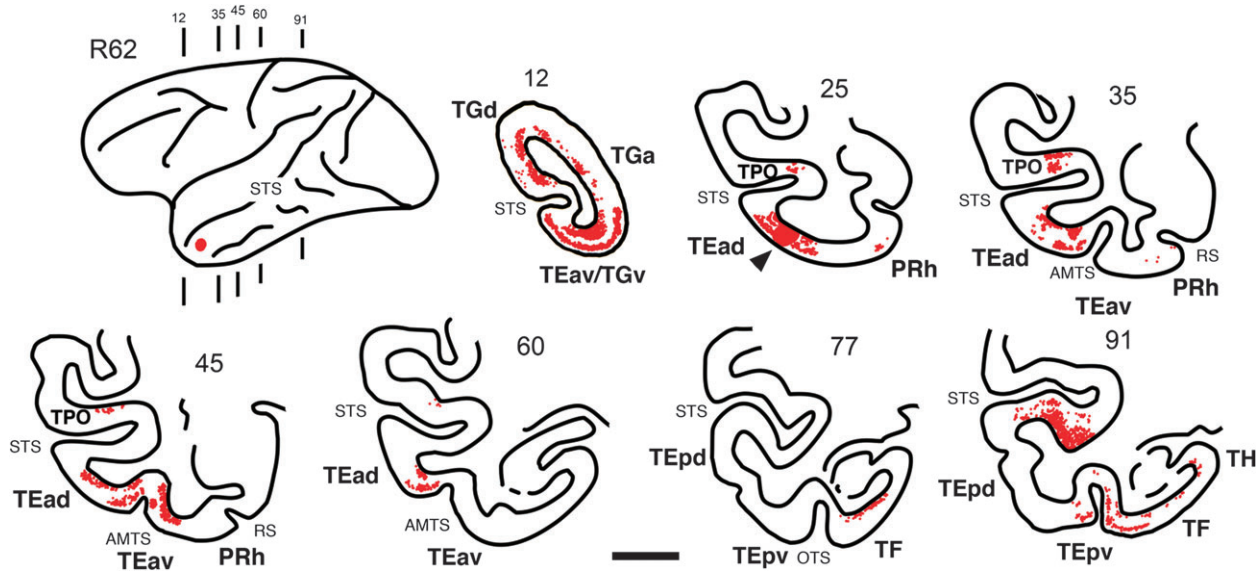

Figure 9. Schematic left hemisphere and ventral portion of 7 coronal sections showing the location of the injection site anterior in TEad (case R62) and the distribution of Zn+ neurons. Larger numbers are more posterior. Other conventions are the same as in Figure 2*E*. TGd, area TGd; others, see Figure 7. Scale bar, 5 mm.

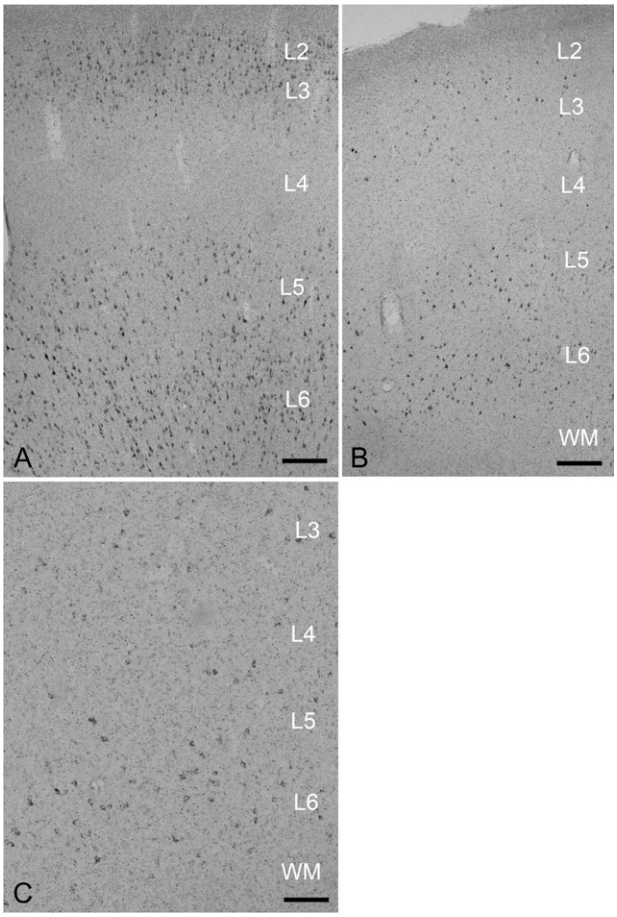

Figure 10. Three fields of Zn+ neurons, labeled by the injection in TEad (case R62). (*A*) Neurons in layers 2, upper 3, 5, and 6 of the temporal pole (Fig. 9, section 12). (*B*) Neurons mainly in layers 5 and 6 of the lower bank of the anterior medial temporal sulcus. Some neurons also occur in the upper layers (Fig. 9, section 45). (*C*) Neurons mainly in the lower layers of the STS, with a few in the upper layers (Fig. 9, section 91). Scale bar: *A*, *C*, 100 μm; *B*, 200 μm.

Consistent with our past results (Miyashita et al. 2007), however, filling was not Golgi-like, and in particular there was no evidence of axonal filling or filling of local collaterals.

Four areas were analyzed: areas V1, V4, TEO, and the depth of the STS. In all 4 areas, there was a mix of terminations that either were positive only for BDA (BDA+/Zn-negative in Table 1) or were positive for both BDA and zinc (BDA+/Zn+ in Table 1). In TEO, the area closest to the injection, 12 of the 19 scored profiles were only BDA+ and 7 were BDA+ and Zn+. In V4, 9 of the 15 profiles were only BDA+ and 6 were both BDA+ and Zn+. In the STS, 4 of the 10 profiles were only BDA+ and 6 were both BDA+ and Zn+. In V1, the area furthest from the injection, profiles labeled for BDA or zinc were less dense. Within this smaller sample in V1, there was a distinct bias for double-labeled profiles, namely 1 of the 5 profiles was only BDA+ and 4 were BDA+ and Zn+.

These data indicate that only a subset of BDA-labeled terminations are positive for zinc. This finding is consistent with our results from sodium selenite injections, where layer 2 feedback projection neurons were zinc negative. In addition, a partial dissociation between BDA+ and Zn+ terminations follows from the respective laminar distributions. That is, consistent with previous reports, BDA-labeled feedback terminations were dense in layers 1a, 1b, and adjoining 2, but Zn+ terminations were sparse in layer 1a (Fig. 12*B*). Portions of single BDA+ fibers could often be followed through both layers 1a and 1b. These might be zinc negative, whereas a subpopulation more closely coinciding with the distribution of Zn+ terminations would be more likely to be Zn+.

Discussion

In general, primary and early sensory areas have low levels of zinc, whereas limbic areas in the temporal lobe, medial interhemispheric surface, and orbitofrontal areas contain higher levels of Zn+ terminations (Carmichael and Price 1994; Pérez-Clausell 1996; Frederickson et al. 2000; Ichinohe and Rockland 2004, 2005). In area V1, Zn+ terminations in layers 3 and 4A form patches that are complementary to thalamocortical terminations, as visualized by cytochrome oxidase (Dyck and Cynader 1993; Dyck et al. 2003).

By using focal injections of sodium selenite, we have determined intrinsic and extrinsic cortical sources of Zn+ terminations to specific cortical sites. For the early visual areas (V1, V4, and TEO), Zn+ projections are correlated with feedback projections. Surprisingly, however, only the component originating from layer 6, but not that from layer 2 or 3, is Zn+. For temporal areas, association intratemporal connections as well as feedback projections were observed to be Zn+. Laminar distribution of neurons in this case appeared similar to what has been reported after standard retrograde tracers, namely layers 2 and 6 for feedback and layers 2, 3, 5, and 6 for associational connections (Rockland and Pandya 1979; Maunsell and Van Essen 1983; Felleman and Van Essen 1991; Suzuki and Amaral 1994; Saleem and Tanaka 1996; Saleem et al. 2000; Ungerleider et al. 2008).

All the injections resulted in intrinsic Zn+ neurons in layer 2. In V1, where the density of Zn+ terminations is lowest, these were limited to the immediate vicinity of the injection. Presumably, the intrinsic Zn+ connections in V1 are predominantly vertical, so that most of the Zn+ neurons in deeper layers would be obscured within the injection site. In V4 and TEO, Zn+ neurons also concentrated in layer 2 but extended further laterally. In these areas, Zn+ neurons were notably absent from layer 3 or 5, although these layers contain abundant intrinsically projecting pyramidal neurons after injections of standard tracers. Finally, the temporal injections all produced extensive label in layer 2 (for 1.5–2.5 mm), a secondary band in layer 6, and scattered Zn+ neurons in layers 3 and 5. None of these intrinsic connections had any discernible patchiness, except that the sparse label in layer 3 of temporal areas showed some periodic fluctuation.

Technical Considerations

Evaluation of these results depends on the reliability and sensitivity of sodium selenite as a tracer. That is, could the absence of Zn+ neurons in certain projections or layers be due to a simple failure of transport? We cite 3 factors that argue against this possibility. First, sodium selenite has been extensively vetted in rodents, with no reports of technical artifacts (Christensen et al. 1992; Casanovas-Aguilar et al. 1995, 1998; Brown and Dyck 2005). Second, Zn+ neurons are detected in distant sites as well as nearby the injection (Ichinohe and Rockland 2005; this study). Third, our results

are consistent with the known pattern of Zn+ terminations (Pérez-Clausell 1996; Ichinohe and Rockland 2005). These are low in layer 4, the recipient layer of feedforward terminations (Rockland and Pandya 1979; Maunsell and Van Essen 1983; Felleman and Van Essen 1991); and our injections in fact revealed absence of Zn+ neurons among feedforward projections. Similarly, Zn+ terminations are dense in layers that receive feedback projections. Both our retrograde labeling and EM results, however, indicate that only a subset of the feedback connections are Zn+. This is consistent with the fact that BDA-labeled feedback terminations extend beyond the zone of Zn+ terminations, which avoid layer 1a. Because we have scanned sections at a relatively close interval (200 μm), we consider that the absence of supragranular labeling is real and not due to observer oversight (see Supplementary Fig. 1). Moreover, comparison of labeled foci after injections of sodium selenite or injections of conventional tracers did not reveal marked differences in density of labeled neurons in temporal area injection cases (see Fig. 11). Thus, we suggest that the absence of retrogradely transported zinc selenite can be take as a reliable indicator that those neurons do not have Zn+ synapses at the injection site.

Functional Significance

The functional significance of our results depends on what happens at particular Zn+ synapses. From the limited experimental data on the physiological properties of long distance cortical synapses, we can expect that Zn+ synapses have distinct voltage dependence, decay kinetics, and receptor subunit–specific pharmacology (in rodent: Kumar and Huguenard 2003). Corticocortical synapses, as assayed in vitro, exhibit either paired-pulse facilitation or inhibition, depending on the combination of pre- and postsynaptic subtypes (see for review: Thomson and Lamy 2007). In the case of Zn+ synapses, the synaptic response may be further influenced by zinc concentration and target identity (Paoletti et al. 2009).

Evidence from in vitro preparations and deprivation experiments has consistently suggested that synaptic zinc has a role in activity-dependent plasticity (Frederickson et al. 2005; Nakashima and Dyck 2009). The potential mechanisms are numerous and varied, including translocation into postsynaptic neurons (Li et al. 2001), interaction with NMDA receptors (Rachline et al. 2005), activation of Trk receptors (Huang et al. 2008), and, still hypothetical, an important role in the modulation of the postsynaptic density (Gundelfinger et al. 2006). Finally, although most discussions have emphasized the potential positive influences of zinc on synaptic plasticity, another idea is that the release of zinc may help to stabilize synapses, which are otherwise predisposed to modifications in synaptic strength, by a high density of NMDA receptors or other factors (Slomianka 1992; Ueno et al. 2002; Paoletti et al. 2009).

The location of Zn+ neurons and the distribution of Zn+ terminations suggest a preferential association of zinc with feedback and lateral connections; and our combined EM-BDA results corroborate that a subpopulation of feedback synapses are Zn+. Feedback and lateral connections have consistently been differentiated from feedforward, layer 4–targeting inputs, as

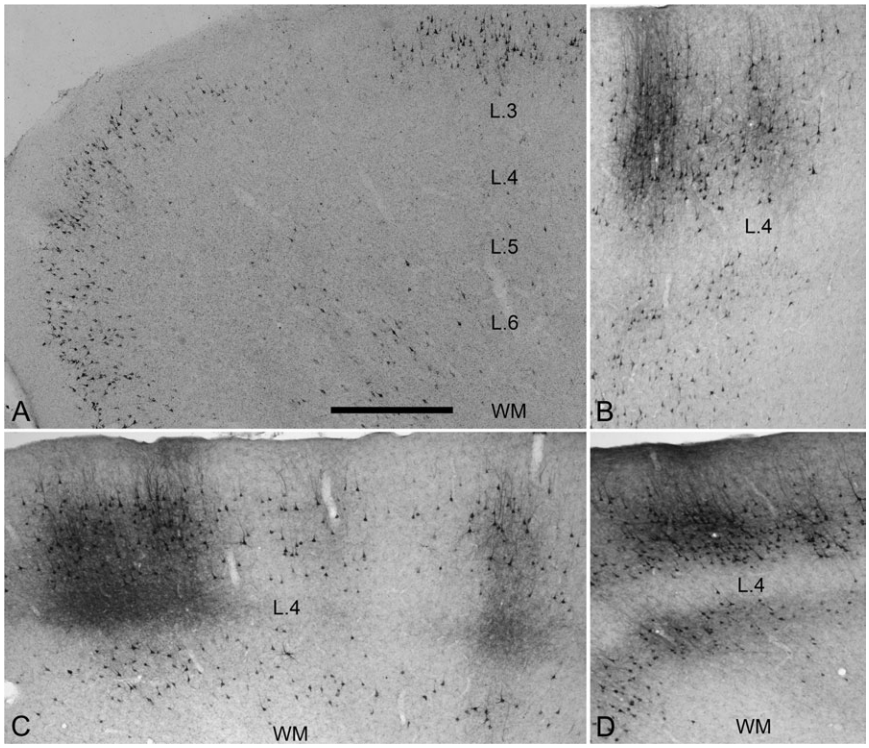

Figure 11. Comparison of labeling after injections of sodium selenite (section 33, from case 299: injection in TEav/perirhinal border) and injections of cholera toxin B-subunit (CTB)-Alexa 488 (DAB reaction, see Borra et al. 2010). (*A*) Zn+ neurons are mainly in layer 2, but some also are evident in the deeper layers. This section is anterior to the injection (lateral is at the top and the lower bank of AMTS is at the left). (*B–D*) Three fields of neurons labeled by an injection of CTB-Alexa 488 in area TEad. Note the preferential location of labeled neurons in layers 3 and 5. Some occur in layer 2, but the greater number of neurons is in layer 3. (*B*) Neurons in the lower bank of the STS occur in layers 3, 5, and 6. (*C*) Neurons anterior to the injection (in TEad) are also located in layers 3, 5, and 6. Dense anterograde label is apparent in layer 4. (*D*) Posterior to the injection, in TEpd, labeled neurons are dense in layer 3, but some are located in layer 5. Anterograde labeling is discernible in layers 1 and 5, and collateral labeling in layer 3. Scale bar: 500 μm.

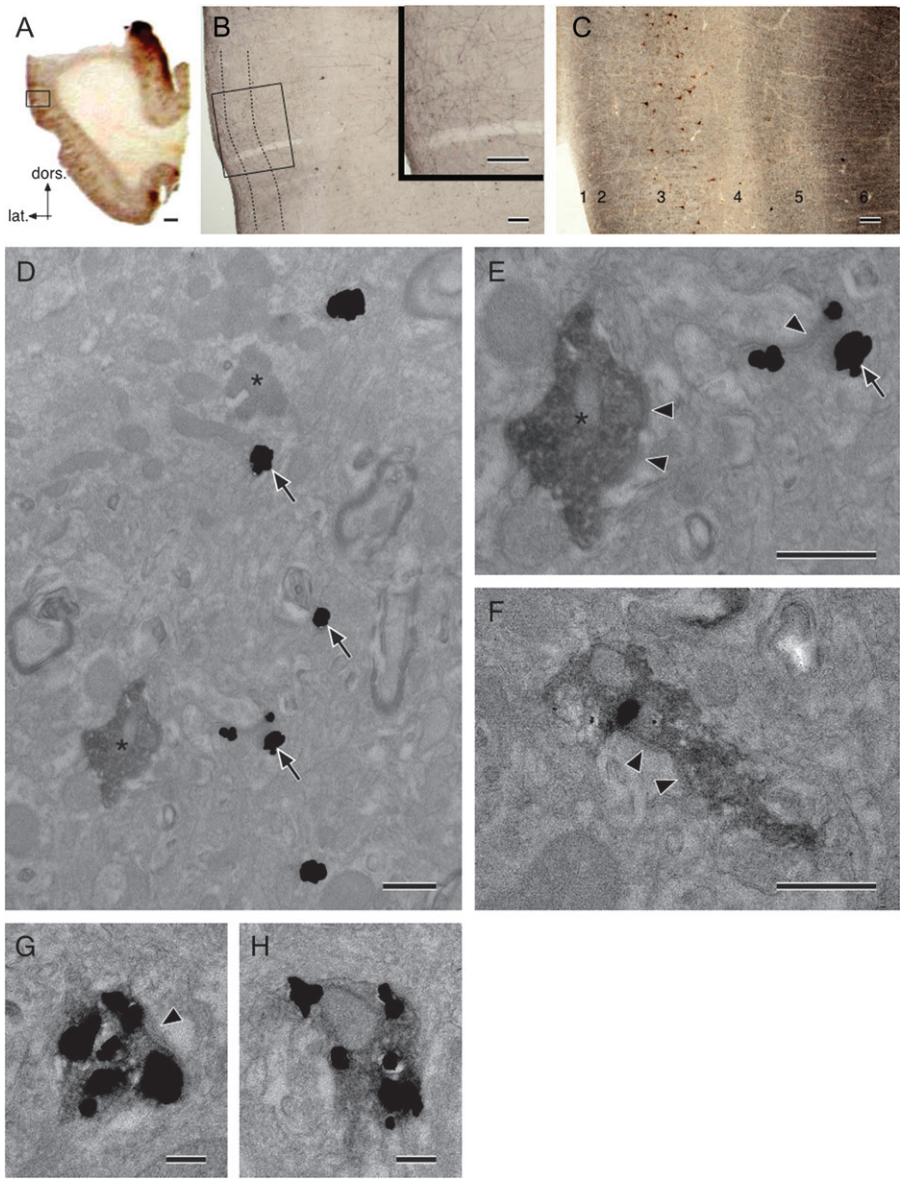

Figure 12. Flat-embedded tissue (*A–C*) and electron micrographs of BDA+, Zn+, and BDA+/Zn+ synapses in area TEO (*D–F*), STS (*G*), and V1 (*H*). BDA was injected in area TEpd, and Zn+ synapses were visualized by silver grains, precipitated by sodium sulfide in the perfusate. (*A–C*) Light micrographs of area TEO showing the region of interest. (*A*) Vibratome-cut section reacted for BDA only. Framed area is magnified in (*B*). (*B*) BDA-labeled terminations are evident in layers 1 and upper 2 (dashed lines indicate layer 2 and lower layer 1). The inset shows further detail at higher magnification. BDA-labeled feedback terminations do not show any sublaminar preference. (*C*) Section adjacent to the one in (*B*), which was reacted for both BDA and zinc. Dense zinc labeling was found in layers 1b, 2, 5A, and 6. A few pyramidal cells, retrogradely labeled by BDA, are evident in layer 3. Numbers 1–6 indicate cortical layers. (*D–H*) Electron micrographs of BDA+, Zn+, and BDA+/Zn+ synapses from the layer 1/2 border. (*D*) Low-power micrograph, from area TEO, with several Zn+ synapses (arrows), and BDA-labeled synapses (asterisks). (*E*) Higher magnification from (*D*) showing a BDA+/Zn-negative synapse (asterisk) and Zn+/BDA-negative synapse (arrow). The Zn+ profile contacts a spine-like structure, and there is a distinct postsynaptic density. (*F*) A BDA+ profile in area TEO, which is also Zn+. (*G–H*) Synapses in the STS (*G*) and V1 (*H*), both of which are clearly positive for BDA and zinc. BDA-positive profiles are filled with presynaptic vesicles (cf. solely BDA+ profiles in *D* and *E*). Arrowheads in *E*, *F*, *G* indicate postsynaptic densities. dors., dorsal; lat., lateral. Scale bar: *A*, 1 mm; *B*, *C*, inset, 100 μm; *D–F*, 0.5 μm; *G*, *H*, 0.2 μm.

exhibiting more rapid or differential plasticity (Crair and Malenka 1995; Feldman et al. 1998; Glazewski et al. 1998; Trachtenberg et al. 2000; Jiang et al. 2007). In this respect, it is interesting to note that feedback inputs from higher visual areas to V1 have been discussed as accelerating and strengthening perceptual learning (see for review: Gilbert and Sigman 2007; Kiper et al. 2007). Feedback signals from medial temporal perirhinal areas are thought to mediate the visual associative mnemonic codes of inferotemporal neurons (Higuchi and Miyashita 1996).

More unexpected is the selective absence of synaptic zinc in feedback-projecting neurons from layer 2 to early visual areas. This is particularly puzzling because layer 2 contains abundant intrinsically projecting Zn+ neurons. The most plausible explanation is that layer 2 contains a mixed population of Zn+ intrinsically projecting and Zn negative extrinsically projecting neurons. This dissociation seems to occur preferentially in the early visual areas, in contrast with temporal association areas.

Another indication of important distinctions between feedback-projecting neurons in layers 2 and 6 is from investigations of collateralization. That is, after retrograde dye injections in areas V1 and V4, a few neurons in layer 6 of V2

(3.4%) were double-labeled. By contrast, there were almost no double-labeled neurons (0.67%) in the supragranular layers of V2 (Markov et al. 2007).

Many markers are specific for layer 2 or 6 but not both. Gene expression profiles are often layer specific, for example, in primate, "retinol-binding protein" expression is dense only in the uppermost layers in V2, V4, and TEO (Komatsu et al. 2005). *Nurr1* is highly expressed in layer 6A but not in the upper layers (Watakabe et al. 2007). A novel aspect of our results, given the proposed actions of zinc, is the implication of significant pathway and laminar differences in relation to synaptic properties.

Projectional Subpopulations

Previous investigations have demonstrated the area and laminar distribution of Zn+ terminations in primate cortex. As far as we know, there have been no reports of the distribution of Zn+ cortical neurons by focal injections, but several similar studies have been carried out for amygdalocortical projections. That is, focal injections of sodium selenite in temporal areas revealed Zn+ neurons in the basolateral nucleus (Ichinohe and Rockland 2005); and EM inspection of BDA-labeled amygdalocortical terminations has confirmed that these are Zn+ (Miyashita et al. 2007). EM analysis of amygdalocortical projections to medial prefrontal cortex revealed that all the inspected BDA-labeled terminations, not just a subset, were Zn+. Consistent with this finding, there is tight correspondence between the laminar distribution of amygdalocortical and Zn+ terminations, both of which target layer 1b and the layer 1/2 border (Freese and Amaral 2006). The proportion of Zn+ neurons may be species specific as a comparable study in the rat reported that only 35% of basolateral neurons, projecting to the medial prefrontal cortex, contained zinc (Cunningham et al. 2007).

Previous studies, using other criteria than the presence or absence of synaptic zinc, have reported subpopulations within a projection system. Thicker myelinated versus thinner unmyelinated axon subpopulations are commonly identified within a given projection, for example, there is a recent report concerning corticocollicular projections in the cat (Fuentes-Santamaria et al. 2009). Particularly relevant to the present results, V2 feedback axons to V1 are reported as thick, myelinated, heavily branched, and bearing clusters of terminations or thin, unmyelinated, and uniformly covered with boutons (Anderson and Martin 2009). An earlier study, where retrogradely labeled neurons were double-reacted for neurofilament protein, reported that neurofilament-containing feedback-projecting neurons in areas V4 and MT are more frequent in layers 5 and 6 than in layers 2 and 3 (Hof et al. 1996).

The observation that some projections are entirely Zn negative is borne out by studies in rodent, for example, projections from the cingulate, retrosplenial, perirhinal, and lateral entorhinal cortices to mouse visual cortex are Zn negative (Garrett et al. 1992). The finding that Zn+ terminations can originate from only some of the layers giving rise to a given projection has also been repeatedly described in rodent. In the rat visual cortex, Zn+ callosally projecting neurons occur in layers 2, 3, and 6 but not in layer 4 or 5 (Casanovas-Aguilar et al. 1995). Sodium selenite injections in mouse barrel cortex result in Zn+ neurons in layers 2, 3, and 6. This is a more limited distribution than that seen after injections of cholera toxin (Brown and Dyck 2005). Zn+ cortical projections from hippocampal CA1, in both rodents (Slomianka 1992) and monkeys (Ichinohe and Rockland 2005), preferentially originate from pyramidal neurons in the upper stratum. It is currently unknown whether Zn+ and Zn-negative components have separate postsynaptic targets.

Subpopulations within specific projections are an excellent target for future functional investigations into synaptic properties and connectional interactions (Cardin et al. 2009; Petreanu et al. 2009).

Funding

Brain Science Institute, RIKEN; Grant-in-Aid for Scientific Research on Priority Areas "System study on higher order brain functions" and "Elucidation of neural network function in the brain" (18020032, 20021033) and Grant-in-Aid for Scientific Research on Innovative Areas "Face perception and recognition" (21119502) from the Ministry of Education, Culture, Sports, Science and Technology of Japan; Joint Research Programs of the National Institute for Basic Biology, Japan, and of the National Institute for Physiological Science, Japan; Grant for Hirosaki University Institutional Research.

Supplementary Material

Supplementary material can be found at: http://www.cercor.oxfordjournals.org/.

Notes

We thank Hiromi Mashiko and Yoshiko Abe for excellent technical support; Michiko Fujisawa for assistance with manuscript preparation; and James Hyde for assistance with the figures. *Conflict of Interest*: None declared.

References

Anderson JC, Martin KA. 2009. The synaptic connections between cortical areas V1 and V2 in macaque monkey. J Neurosci. 29:11283–11293.

Baizer JS, Ungerleider LG, Desimone R. 1991. Organization of visual inputs to the inferior temporal and posterior parietal cortex in macaques. J Neurosci. 11:168–190.

Barone P, Batardiere A, Knoblauch K, Kennedy H. 2000. Laminar distribution of neurons in extrastriate areas projecting to visual areas V1 and V4 correlates with the hierarchical rank and indicates the operation of a distance rule. J Neurosci. 20:3263–3281.

Born RT, Bradley DC. 2005. Structure and function of visual area MT. Annu Rev Neurosci. 28:157–189.

Borra E, Ichinohe N, Sato T, Tanifuji M, Rockland KS. 2010. Cortical connections to area TE in monkey: hybrid modular and distributed organization. Cereb Cortex. 20:257–270.

Brown CE, Dyck RH. 2003. An improved method for visualizing the cell bodies of zincergic neurons. J Neurosci Methods. 129:41–47.

Brown CE, Dyck RH. 2004. Distribution of zincergic neurons in the mouse forebrain. J Comp Neurol. 479:156–167.

Brown CE, Dyck RH. 2005. Retrograde tracing of the subset of afferent connections in mouse barrel cortex provided by zincergic neurons. J Comp Neurol. 486:48–60.

Cardin JA, Carlén M, Meletis K, Knoblich U, Zhang F, Deisseroth K, Tsai LH, Moore CI. 2009. Driving fast-spiking cells induces gamma rhythm and controls sensory responses. Nature. 459:663–667.

Carmichael ST, Price JL. 1994. Architectonic subdivision of the orbital and medial prefrontal cortex in the macaque monkey. J Comp Neurol. 346:366–402.

Casanovas-Aguilar C, Christensen MK, Reblet C, Martínez-García F, Pérez-Clausell J, Bueno-López JL. 1995. Callosal neurones give rise to zinc-rich boutons in the rat visual cortex. Neuroreport. 6:497–500.

Casanovas-Aguilar C, Miró-Bernié N, Pérez-Clausell J. 2002. Zinc-rich neurones in the rat visual cortex give rise to two laminar segregated systems of connections. Neuroscience. 110:445–458.
Casanovas-Aguilar C, Reblet C, Pérez-Clausell J, Bueno-López JL. 1998. Zinc-rich afferents to the rat neocortex: projections to the visual cortex traced with intracerebral selenite injections. J Chem Neuroanat. 15:97–109.
Christensen MK, Frederickson CJ, Danscher G. 1992. Retrograde tracing of zinc-containing neurons by selenide ions: a survey of seven selenium compounds. J Histochem Cytochem. 40: 575–579.
Crair MC, Malenka RC. 1995. A critical period for long-term potentiation at thalamocortical synapses. Nature. 375:325–328.
Cunningham MG, Ames HM, Christensen MK, Sorensen JC. 2007. Zincergic innervation of medial prefrontal cortex by basolateral projection neurons. Neuroreport. 18:531–535.
Danscher G, Nørgaard JO, Baatrup E. 1987. Autometallography: tissue metals demonstrated by a silver enhancement kit. Histochemistry. 86:465–469.
De Biasi S, Bendotti C. 1998. A simplified procedure for the physical development of the sulphide silver method to reveal synaptic zinc in combination with immunocytochemistry at light and electron microscopy. J Neurosci Methods. 79:87–96.
Distler C, Boussaoud D, Desimone R, Ungerleider LG. 1993. Cortical connections of inferior temporal area TEO in macaque monkeys. J Comp Neurol. 334:125–150.
Doty RW. 1983. Nongeniculate afferents to striate cortex in macaques. J Comp Neurol. 218:159–173.
Dyck RH, Chaudhuri A, Cynader MS. 2003. Experience-dependent regulation of the zincergic innervation of visual cortex in adult monkeys. Cereb Cortex. 13:1094–1109.
Dyck RH, Cynader MS. 1993. An interdigitated columnar mosaic of cytochrome oxidase, zinc, and neurotransmitter-related molecules in cat and monkey visual cortex. Proc Natl Acad Sci U S A. 90:9066–9069.
Feldman DE, Nicoll RA, Malenka RC, Isaac JT. 1998. Long-term depression at thalamocortical synapses in developing rat somatosensory cortex. Neuron. 21:347–357.
Felleman DJ, Van Essen DC. 1991. Distributed hierarchical processing in the primate cerebral cortex. Cereb Cortex. 1:1–47.
Frederickson CJ, Koh JY, Bush AI. 2005. The neurobiology of zinc in health and disease. Nat Rev Neurosci. 6:449–462.
Frederickson CJ, Suh SW, Silva D, Frederickson CJ, Thompson RB. 2000. Importance of zinc in the central nervous system: the zinc-containing neuron. J Nutr. 130:1471S–1483S.
Freese JL, Amaral DG. 2006. Synaptic organization of projections from the amygdala to visual cortical areas TE and V1 in the macaque monkey. J Comp Neurol. 496:655–667.
Fuentes-Santamaria V, Alvarado JC, McHaffie JG, Stein BE. 2009. Axon morphologies and convergence patterns of projections from different sensory-specific cortices of the anterior ectosylvian sulcus onto multisensory neurons in the cat superior colliculus. Cereb Cortex. 19:2902–2915.
Fujita I, Fujita T. 1996. Intrinsic connections in the macaque inferior temporal cortex. J Comp Neurol. 368:467–486.
Garrett B, Sørensen JC, Slomianka L. 1992. Fluoro-Gold tracing of zinc-containing afferent connections in the mouse visual cortices. Anat Embryol (Berl). 185:451–459.
Gilbert CD, Sigman M. 2007. Brain states: top-down influences in sensory processing. Neuron. 54:677–696.
Glazewski S, Herman C, McKenna M, Chapman PF, Fox K. 1998. Long-term potentiation in vivo in layers II/III of rat barrel cortex. Neuropharmacology. 37:581–592.
Gundelfinger ED, Boeckers TM, Baron MK, Bowie JU. 2006. A role for zinc in postsynaptic density asSAMbly and plasticity? Trends Biochem Sci. 31:366–373.
Higuchi S, Miyashita Y. 1996. Formation of mnemonic neuronal responses to visual paired associates in inferotemporal cortex is impaired by perirhinal and entorhinal lesions. Proc Natl Acad Sci U S A. 93:739–743.
Hof PR, Ungerleider LG, Webster MJ, Gattass R, Adams MM, Sailstad CA, Morrison JH. 1996. Neurofilament protein is differentially distributed in subpopulations of corticocortical projection neurons in the macaque monkey visual pathways. J Comp Neurol. 376: 112–127.
Huang YZ, Pan E, Xiong ZQ, McNamara JO. 2008. Zinc-mediated transactivation of TrkB potentiates the hippocampal mossy fiber-CA3 pyramid synapse. Neuron. 57:546–558.
Ichinohe N, Hyde J, Matsushita A, Ohta K, Rockland KS. 2008. Confocal mapping of cortical inputs onto identified pyramidal neurons. Front Biosci. 13:6354–6373.
Ichinohe N, Potapov D, Rockland KS. 2006. Transient synaptic zinc-positive thalamocortical terminals in the developing barrel cortex. Eur J Neurosci. 24:1001–1010.
Ichinohe N, Rockland KS. 2004. Region specific micromodularity in the uppermost layers in primate cerebral cortex. Cereb Cortex. 14:1173–1184.
Ichinohe N, Rockland KS. 2005. Zinc-enriched amygdalo- and hippocampo-cortical connections to the inferotemporal cortices in macaque monkey. Neurosci Res. 53:57–68.
Jiang B, Treviño M, Kirkwood A. 2007. Sequential development of long-term potentiation and depression in different layers of the mouse visual cortex. J Neurosci. 27:9648–9652.
Kiper D, Martin KA, Scherberger H. 2007. Cortical plasticity: a view from nonhuman primates. Neurodegener Dis. 4:34–42.
Komatsu Y, Watakabe A, Hashikawa T, Tochitani S, Yamamori T. 2005. Retinol-binding protein gene is highly expressed in higher-order association areas of the primate neocortex. Cereb Cortex. 15: 96–108.
Kondo H, Saleem KS, Price JL. 2003. Differential connections of the temporal pole with the orbital and medial prefrontal networks in macaque monkeys. J Comp Neurol. 465:499–523.
Kondo H, Saleem KS, Price JL. 2005. Differential connections of the perirhinal and parahippocampal cortex with the orbital and medial prefrontal networks in macaque monkeys. J Comp Neurol. 493:479–509.
Kumar SS, Huguenard JR. 2003. Pathway-specific differences in subunit composition of synaptic NMDA receptors on pyramidal neurons in neocortex. J Neurosci. 23:10074–10083.
Lavenex P, Suzuki WA, Amaral DG. 2002. Perirhinal and parahippocampal cortices of the macaque monkey: projections to the neocortex. J Comp Neurol. 447:394–420.
Lavenex P, Suzuki WA, Amaral DG. 2004. Perirhinal and parahippocampal cortices of the macaque monkey: Intrinsic projections and interconnections. J Comp Neurol. 472:371–394.
Li Y, Hough CJ, Frederickson CJ, Sarvey JM. 2001. Induction of mossy fiber → Ca3 long-term potentiation requires translocation of synaptically released Zn^{2+}. J Neurosci. 21:8015–8025.
Markov NT, Chameau P, Barone P, Autran D, Giroud P, Benkerri S, Dehay C, Kennedy H. 2007. Feedforward and feedback pathways in the primate cortex show sharp anatomical segregation and some morphological distinction. San Diego (CA): Society for Neuroscience (Program No. 280.2; 2007 Neuroscience Meeting Planner. Online).
Martin-Elkins CL, Horel JA. 1992. Cortical afferents to behaviorally defined regions of the inferior temporal and parahippocampal gyri as demonstrated by WGA-HRP. J Comp Neurol. 321: 177–192.
Maunsell JHR, Van Essen DC. 1983. The connections of the middle temporal visual area (MT) and their relationship to a cortical hierarchy in the macaque monkey. J Neurosci. 3:2563–2586.
Miyashita T, Ichinohe N, Rockland KS. 2007. Differential modes of termination of amygdalothalamic and amygdalocortical projections in the monkey. J Comp Neurol. 502:309–324.
Nakashima AS, Dyck RH. 2009. Zinc and cortical plasticity. Brain Res Rev. 59:347–373.
Paoletti P, Vergnano AM, Barbour B, Casado M. 2009. Zinc at glutamatergic synapses. Neuroscience. 158:126–136.
Pérez-Clausell J. 1996. Distribution of terminal fields stained for zinc in the neocortex of the rat. J Chem Neuroanat. 11:99–111.

Petreanu L, Mao T, Sternson SM, Svoboda K. 2009. The subcellular organization of neocortical excitatory connections. Nature. 457:1142–1145.
Rachline J, Perin-Dureau F, Le Goff A, Neyton J, Paoletti P. 2005. The micromolar zinc-binding domain on the NMDA receptor subunit NR2B. J Neurosci. 25:308–317.
Rockland KS, Pandya DN. 1979. Laminar origins and terminations of cortical connections of the occipital lobe in the rhesus monkey. Brain Res. 179:3–20.
Rockland KS, Saleem KS, Tanaka K. 1994. Divergent feedback connections from areas V4 and TEO in the macaque. Vis Neurosci. 11:579–600.
Rockland KS, Van Hoesen GW. 1994. Direct temporal-occipital feedback connections to striate cortex (V1) in the macaque monkey. Cereb Cortex. 4:300–313.
Saleem KS, Logothetis NK. 2007. A combined MRI and histology atlas of the rhesus monkey brain (spiral-bound). London: Academic Press.
Saleem KS, Price JL, Hashikawa T. 2007. Cytoarchitectonic and chemoarchitectonic subdivisions of the perirhinal and parahippocampal cortices in macaque monkeys. J Comp Neurol. 500:973–1006.
Saleem KS, Suzuki W, Tanaka K, Hashikawa T. 2000. Connections between anterior inferotemporal cortex and superior temporal sulcus regions in the macaque monkey. J Neurosci. 20: 5083–5101.
Saleem KS, Tanaka K. 1996. Divergent projections from the anterior inferotemporal area TE to the perirhinal and entorhinal cortices in the macaque monkey. J Neurosci. 16:4757–4775.
Saleem KS, Tanaka K, Rockland KS. 1993. Specific and columnar projection from area TEO to TE in the macaque inferotemporal cortex. Cereb Cortex. 3:454–464.
Seltzer B, Pandya DN. 1989. Intrinsic connections and architectonics of the superior temporal sulcus in the rhesus monkey. J Comp Neurol. 290:451–471.
Sensi SL, Paoletti P, Bush AI, Sekler I. 2009. Zinc in the physiology and pathology of the CNS. Nat Rev Neurosci. 10:780–791.
Sincich LC, Horton JC. 2005. The circuitry of V1 and V2: integration of color, form, and motion. Annu Rev Neurosci. 28:303–326.
Slomianka L. 1992. Neurons of origin of zinc-containing pathways and the distribution of zinc-containing boutons in the hippocampal region of the rat. Neuroscience. 48:325–352.
Slomianka L, Danscher G, Frederickson CJ. 1990. Labeling of the neurons of origin of zinc-containing pathways by intraperitoneal injections of sodium selenite. Neuroscience. 38: 843–854.
Smart TG, Hosie AM, Miller PS. 2004. Zn^{2+} ions: modulators of excitatory and inhibitory synaptic activity. Neuroscientist. 10:432–442.
Suzuki WA, Amaral DG. 2003a. Where are the perirhinal and parahippocampal cortices? A historical overview of the nomenclature and boundaries applied to the primate medial temporal lobe. Neuroscience. 120:893–906.
Suzuki WA, Amaral DG. 2003b. Perirhinal and parahippocampal cortices of the macaque monkey: cytoarchitectonic and chemoarchitectonic organization. J Comp Neurol. 463:67–91.
Suzuki WA, Amaral DG. 1994. Perirhinal and parahippocampal cortices of the macaque monkey: cortical afferents. J Comp Neurol. 350:497–533.
Thomson AM, Lamy C. 2007. Functional maps of neocortical local circuitry. Front Neurosci. 1:19–42.
Trachtenberg JT, Trepel C, Stryker MP. 2000. Rapid extragranular plasticity in the absence of thalamocortical plasticity in the developing primary visual cortex. Science. 287:2029–2032.
Ueno S, Tsukamoto M, Hirano T, Kikuchi K, Yamada MK, Nishiyama N, Nagano T, Matsuki N, Ikegaya Y. 2002. Mossy fiber Zn^{2+}spillover modulates heterosynaptic N-methyl-D-aspartate receptor activity in hippocampal CA3 circuits. J Cell Biol. 158:215–220.
Ungerleider LG, Galkin TW, Desimone R, Gattass R. 2008. Cortical connections of area V4 in the macaque. Cereb Cortex. 18: 477–499.
Watakabe A, Ichinohe N, Ohsawa S, Hashikawa T, Komatsu Y, Rockland KS, Yamamori T. 2007. Comparative analysis of layer-specific genes in mammalian neocortex. Cereb Cortex. 17: 1918–1933.
Webster MJ, Bachevalier J, Ungerleider LG. 1994. Connections of inferior temporal areas TEO and TE with parietal and frontal cortex in macaque monkeys. Cereb Cortex. 4:470–483.
Webster MJ, Ungerleider LG, Bachevalier J. 1991. Connections of inferior temporal areas TE and TEO with medial temporal-lobe structures in infant and adult monkeys. J Neurosci. 11:1095–1116.
Wong P, Kaas JH. 2008. Architectonic subdivisions of neocortex in the gray squirrel (*Sciurus carolinensis*). Anat Rec (Hoboken). 291:1301–1333.
Yukie M, Takeuchi H, Hasegawa Y, Iwai E. 1990. Differential connectivity of inferotemporal area TE with the amygdala and the hippocampus in the monkey. In: Iwai E, Mishkin M, editors. Vision, memory, and the temporal lobe. New York: Elsevier. p. 129–135.
Zeki S. 1996. Are areas TEO and PIT of monkey visual cortex wholly distinct from the fourth visual complex (V4 complex)? Proc Biol Sci. 263:1539–1544.